Visual Tracking in Amblyopia: A Continuous Psychophysical Approach

Cheng Li,[1] Yan Yang,[1,2] Jinli Zhu,[1] Yijin Han,[1] Jia He,[1] Jun Wang,[1] Yufan Feng,[1] Junli Yuan,[1] Xiaolin Huang,[1] Renjie Liu,[1] Hanyi Zhang,[1] Xiaowei Ruan,[3,4] and Fang Hou[3,4]

[1]School of Ophthalmology and Optometry and Eye Hospital, Wenzhou Medical University, Wenzhou, China
[2]Civil Aviation General Hospital, Beijing, China
[3]National Engineering Research Center of Ophthalmology and Optometry, Eye Hospital, Wenzhou Medical University, Wenzhou, China
[4]State Key Laboratory of Ophthalmology, Optometry and Vision Science, Eye Hospital, Wenzhou Medical University, Wenzhou, China

Correspondence: Fang Hou, 270 Xueyuan Xi Road, Room 1707 Building 2, Wenzhou, Zhejiang 325027, China; houf@mail.eye.ac.cn.

Received: November 28, 2023
Accepted: April 10, 2024
Published: May 3, 2024

Citation: Li C, Yang Y, Zhu J, et al. Visual tracking in amblyopia: A continuous psychophysical approach. *Invest Ophthalmol Vis Sci.* 2024;65(5):7. https://doi.org/10.1167/iovs.65.5.7

Purpose. This study aimed to explore the underlying mechanisms of the observed visuomotor deficit in amblyopia.

Methods. Twenty-four amblyopic (25.8 ± 3.8 years; 15 males) and 22 normal participants (25.8 ± 2.1 years; 8 males) took part in the study. The participants were instructed to continuously track a randomly moving Gaussian target on a computer screen using a mouse. In experiment 1, the participants performed the tracking task at six different target sizes. In experiments 2 and 3, they were asked to track a target with the contrast adjusted to individual's threshold. The tracking performance was represented by the kernel function calculated as the cross-correlation between the target and mouse displacements. The peak, latency, and width of the kernel were extracted and compared between the two groups.

Results. In experiment 1, target size had a significant effect on the kernel peak ($F(1.649, 46.170) = 200.958$, $P = 4.420 \times 10^{-22}$). At the smallest target size, the peak in the amblyopic group was significantly lower than that in the normal group (0.089 ± 0.023 vs. 0.107 ± 0.020, $t(28) = -2.390$, $P = 0.024$) and correlated with the contrast sensitivity function ($r = 0.739$, $P = 0.002$) in the amblyopic eyes. In experiments 2 and 3, with equally visible stimuli, there were still differences in the kernel between the two groups (all Ps < 0.05).

Conclusions. When stimulus visibility was compensated, amblyopic participants still showed significantly poorer tracking performance.

Keywords: amblyopia, visual tracking, contrast sensitivity function, uncertainty, internal noise, continuous psychophysics, cross-correlation

Amblyopia, one of the most common eye diseases in children,[1,2] is a developmental visual disorder, resulting from the abnormal visual experience early in life.[3] It is clinically characterized by reduced best-corrected visual acuity that cannot be attributed directly to any apparent pathologic changes in the eyes.[4] Amblyopia affects the central visual system beginning at the primary visual cortex.[3,5] Patients with amblyopia exhibit a variety of visual deficits, including reduced contrast sensitivity,[6–10] abnormal spatial localization,[11] impaired stereopsis,[12,13] and global motion perception.[14,15]

Besides the visual deficits observed in the laboratory, amblyopic patients also perform significantly worse than normal people in visuomotor control (see Grant and Moseley[16] for a review). For example, by analyzing the key kinematic parameters of the hand movement, people found that both amblyopic children[17] and adults[18] showed prolonged movement execution time and high error rate in grasping household objects (i.e., glue sticks and pill bottles) when viewing with the amblyopic eye and with two eyes. Niechwiej-Szwedo et al.[19] found similar results in patients with strabismic amblyopia. Moreover, they also reported an altered temporal coordination between eye and hand movements in these patients.[20]

The aforementioned studies mainly focused on the clinical significance of the effect of amblyopia on visuomotor control. Because visuomotor processing involves integration of sensory (vision, proprioception) information and the coordination of vision and motor processes,[21–23] without systematic manipulation of visual input, it is difficult to understand the exact mechanisms underlying the observed visuomotor deficit in amblyopia.

The continuous psychophysical paradigm, a newly developed computer-based method that allows precise manipulation of visual input,[24–27] could serve a potential tool to investigate the visuomotor control. By asking participants to continuously track a stimulus varying in certain feature space during a long time, the paradigm generates

high-throughput time-series data enables us to perform cross-correlation analysis to relate the behavioral response to the input[28–33] and to reveal the temporal dynamics of the biological system. It has been demonstrated that the paradigm can provide the same measure as the classic trial-based forced-choice paradigm with a higher efficiency.[24,26] Thus, it is very suitable for studies on clinical populations and children, who often have difficulties undergoing long testing sessions.

In this study, we investigated the visuomotor control in amblyopia using a continuous tracking paradigm with three separate experiments. Both amblyopic and normal participants tracked a randomly moving Gaussian target on a computer screen using a mouse. In experiment 1, participants performed the tracking task under six different stimulus conditions. We validated the tracking paradigm by examining the relationship between the tracking performance and target location uncertainty. In experiment 2, we first measured the detection threshold for 150-ms random walk motion in both groups and then measured the tracking performance at their respective thresholds. Considering the potential difference in motion integration time between the two groups, in experiment 3, we asked participants to track a target at their individual motion detection threshold measured with a 500-ms duration.

Methods

Participants

Twenty-four amblyopic (A1–A24; 25.8 ± 3.8 years; 15 males) and 22 normal participants (N1–N22; 25.8 ± 2.1 years; 8 males) were recruited in the study. Participants A1 to A15 and N1 to N15 took part in experiment 1. Participants A2, A3, A5, A6, A7, A8, A12, A13, A14, and A16 to A21 and N2 to N6, N9, and N14 to N22 took part in experiment 2. Participants A2, A3, A5, A6, and A22 to A24 and N2, N3, N5, N15, N18, N19, and N22 took part in experiment 3.

All amblyopic participants who had been previously diagnosed were recruited at Wenzhou Eye Hospital. The detailed information of the amblyopic participants can be found in Table A1, Appendix A. The age-matched normal participants, with best-corrected normal visual acuity (logMAR ≤0.0), were graduate students at Wenzhou Medical University. The detailed information of the normal participants can be found in Table A2, Appendix A. All participants underwent comprehensive ophthalmologic and optometric examinations conducted by the first author, LC. All participants were right-handed.

The experiment protocol adhered to the guidelines of the Declaration of Helsinki and was approved by the institutional review board of human subject research of the Eye Hospital, Wenzhou Medical University. Informed consent was obtained from each participant before the experiment.

Apparatus

Eye dominance was determined with the hole-in-card method for the normal participants.[34] Visual acuity (VA) was measured using the early treatment diabetic retinopathy study (ETDRS) chart.[35,36] Stereoacuity was measured using an random dot stereogram chart.[37] Contrast sensitivity function (CSF) was measured using the quick CSF procedure with a two-alternative forced-choice (2AFC) grating orientation identification task.[38–40]

The programs used in the tracking and motion detection experiment were written in MATLAB (MathWorks, Natick, MA, USA) with the Psychtoolbox extension[41] and run on an Intel NUC computer (NUC6i7kYK; Intel Corporation, Santa Clara, CA, USA). The stimuli were displayed on a gamma-corrected monitor (ASUS SWIFT PG278QR; Asustek Computer, Taipei, Taiwan) running at 120 Hz with a resolution of 2560 × 1440 pixels. The monitor has been carefully tuned and calibrated to minimize the typical artifacts associated with liquid crystal displays.[42,43] The background luminance was set to 58.5 cd/m^2. A standard USB mouse was used in the tracking experiment.

Observers viewed the stimuli monocularly at a distance of 1.34 m in a dark room with their best optical correction, if any. The eye not being tested was occluded by an opaque patch. A chinrest was used to maintain head position during the experiment.

Stimuli

The stimuli for tracking were similar to those used in Bonnen et al.[24] The target was a luminance increment with a two-dimensional Gaussian profile (Fig. 1A) embedded in a square field of dynamic Gaussian pixel noise subtended 6.5° (Fig. 1C). The surrounding area of the noise field was set to the gray background during the entire experiment. In each tracking trial, the target started at the center of the noise field and moved according to a random walk (Brownian) process for 20 seconds (Fig. 1C). The location of the target was updated every two frames (16.7 ms). The target displacements in the horizontal and vertical directions between two consecutive updates were drawn independently from a Gaussian distribution with a mean of 0 and a standard deviation of 0.02°. Each noise element of the noise field subtended 0.02° × 0.02°, the RMS contrast of which was independently drawn from Gaussian distribution with a zero mean and 0.134 standard deviation and updated every two frames. The mouse cursor was indicated by a red dot with a 0.08° diameter, the location of which was also updated every two frames.

In experiment 1, we attempted to investigate how the performance of the tracking paradigm was affected by the visual input by manipulating the target location uncertainty. The luminance of the target was varied with its size so that the luminous flux (the volume under the Gaussian) was constant for all target sizes. Six different target sizes, as represented by the standard deviation of the Gaussian, 11, 13, 17, 21, 25, and 29 arcmin, were used (Fig. 1B). The Weber contrast of the target at six different sizes was 1.0, 0.716, 0.419, 0.274, 0.194, and 0.144, respectively. This design used the property that, for Gaussian targets, the probability of the target center being at a specific location is directly proportional to the luminance value at that location. The constant luminous flux constraint is equivalent to keep the total probability in space constant for all six conditions. All targets were visible. The spatial frequency range of the six targets was less or around 1 cpd (Fig. B1, Appendix B), where the amblyopic participants showed minimum or no reduction in contrast sensitivity (Fig. C2, Appendix C). The target was kept the same during a tracking trial.

In experiment 2, a two-interval forced-choice (2IFC) task was used to measure the Weber threshold for the random walk motion detection. The stimulus was either a static or randomly walking Gaussian luminance increment with the size of 11 arcmin. The static stimulus was presented at

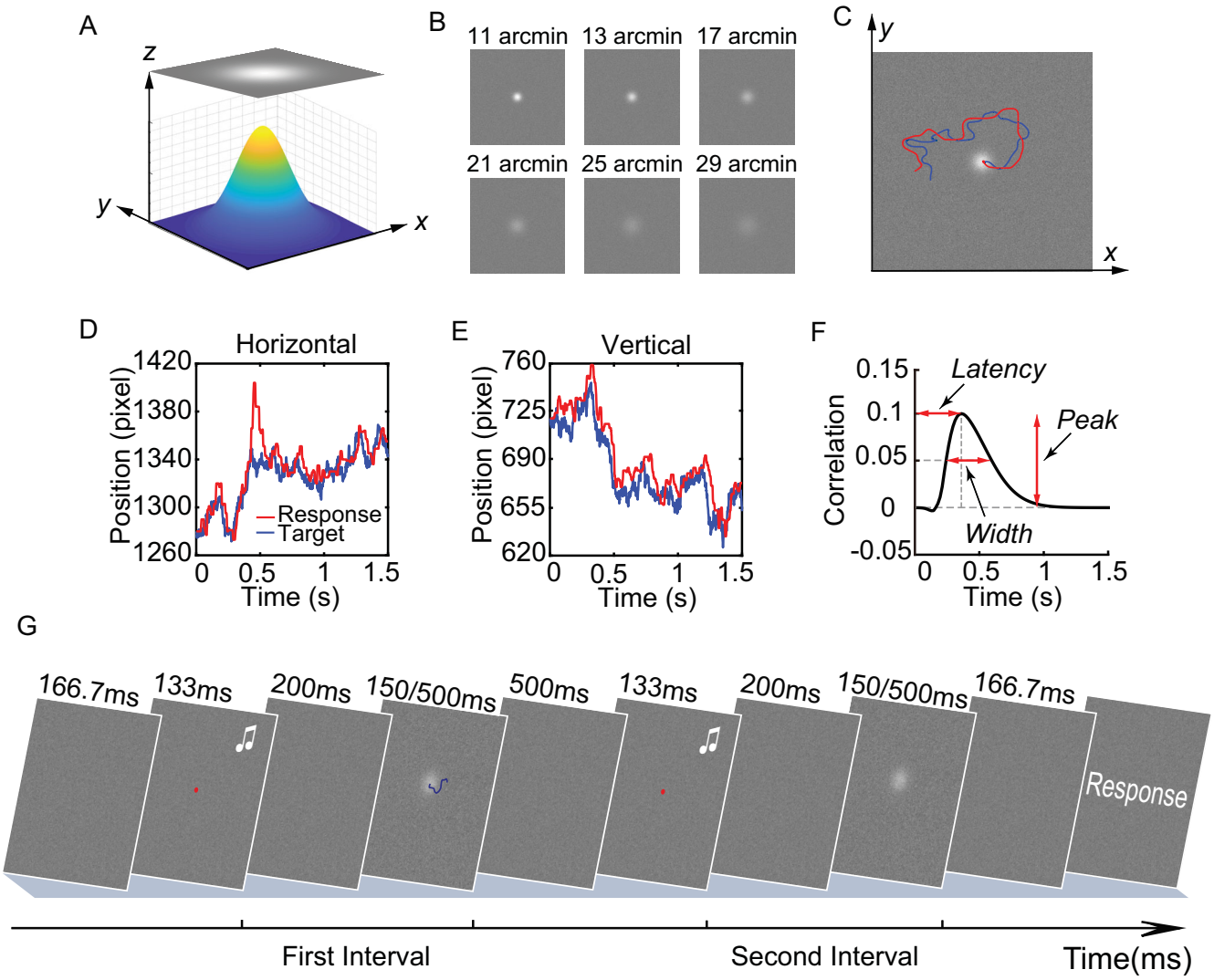

Figure 1. (**A**) The target for tracking was a luminance increment with a Gaussian profile. (**B**) The images of six targets used in experiment 1. (**C**) The target moved randomly according to a Brownian process in a dynamic noise field. Participants were instructed to use the mouse cursor to continuously track the center of the target. The *blue and red lines* represent the example trajectories of the target and mouse cursor, respectively. In the actual experiment, the *blue and red lines* were not visible. (**D**) The horizontal components of the trajectories for the target (*blue*) and cursor (*red*) are plotted against time, respectively. (**E**) The vertical components of the trajectories for the target (*blue*) and cursor (*red*) are plotted against time, respectively. (**F**) The tracking kernel function is calculated as the cross-correlation between the displacements of the target and mouse cursor. The peak, latency, and width of the kernel estimated from the best-fit five-parameter model (Equation (1)) are shown. (**G**) The two-interval forced-choice motion detection task used in experiments 2 and 3. In this demonstration, the randomly moving target is presented in the first interval. The *blue* trajectory is for illustration only and was not visible in the experiment. The target duration was set to 150 ms in experiment 2 and 500 ms in experiment 3.

the center of the screen, and the motion stimulus always started from the center. The stimulus duration was 150 ms. It has been reported that the temporal integration of the human visual system for motion detection is between 100 and 200 ms.[44–47] The background noise field, which was the same as that in experiment 1, was presented throughout the entire trial. The target for tracking displacements was also the same as that in experiment 1. The random walk speed was drawn from a Gaussian distribution with a mean of 0 and standard deviation of 0.02°. The displacement of the 150-ms (eight-frame) random walk was 0.07° ± 0.037° on average, ranging from 0.001° to 0.25°. This value is within the magnitude of fixation error reported in normal and amblyopic people.[48] The dynamic noise field and the randomly walking stimulus were both updated every 16.7 ms. The target contrast was set to an individual's threshold for the 150-ms motion detection.

In experiment 3, the stimulus in the 2IFC motion detection task was exactly the same as that in experiment 2, except the random walk motion duration was set to 500 ms. The stimulus with a longer duration in the 2-IFC task was more similar to that in the tracking task, which enabled the observer to freely follow the moving target.

Procedure

The participants performed all tasks in the study using either their amblyopic eye (for the amblyopic patients) or the nondominant eye (for the normal participants). In case of

bilateral amblyopia, the eye with inferior visual acuity was chosen.

In the quick CSF test, the visual stimulus was a 133-ms sinewave grating of various spatial frequencies oriented +45° or −45° from vertical. In each trial, the quick CSF procedure selects the most informative stimulus by leveraging the information-theoretic framework and estimates the posterior distribution of the CSF based on the response. More details about the quick CSF procedure can be found elsewhere.[39] The individual CSF and group average CSF can be found in Figures C1 and C2, Appendix C, respectively.

In experiment 1, each participant completed a single session of 120 tracking trials, with 20 trials for each target size. Trials with different target sizes were intermixed randomly. One session took about 50 minutes to finish. Before each tracking trial, the red mouse cursor was presented at the center of a blank display. The trial was initiated by a mouse click. There was a brief tone signaling the beginning of tracking. Participants were asked to track the center of the Gaussian target with the mouse cursor as closely as possible for 20 seconds. The horizontal and vertical coordinates of the target and mouse were recorded every 16.7 ms. There were 1,200 samples of data generated in each trial. The participants were given a short break every 20 trials.

In experiments 2 and 3, the Weber contrast threshold for the random walk motion detection for each participant was first measured using the 2IFC motion detection task. In each trial, there were two successive intervals, separated by 500 ms (Fig. 1G). Each interval began with a brief tone and a 133-ms presentation of a red central fixation point. Then a stimulus display was preceded by a 200-ms blank display. In each interval, there was either a static or a randomly walking Gaussian. The stimulus duration was set to 150 ms in experiment 2 and 500 ms in experiment 3. Participants were asked to indicate which interval contained a "moving" target using the keyboard. A new trial started 333.3 ms after the observer's response. A 3-up, 1-down staircase procedure[49] with 80 trials was used to measure the threshold. A brief sound was played after a correct response. After threshold measurement, the participants completed 30 tracking trials. The target size was set to 11 arcmin, and the contrast was set to an individual's threshold in experiments 2 and 3, respectively.

All participants were given a few practice trials before the experiment to make sure they fully understood the task.

Data Analyses

To quantify the tracking performance, the displacement of the target and mouse cursor at each sampling time point was first calculated as the first-order derivatives of the coordinate data. Then, the cross-correlation between the displacement of target and that of the mouse cursor was calculated to obtain the kernel function for tracking (Fig. 1F). Considering the observer as a linear system with the target displacement as input and the mouse response as output, the cross-correlation between the displacements of the target and mouse is the impulse response function or the kernel of the system,[24,28,33,50] which can fully characterize the system. In a single trial, the horizontal and vertical components of the trajectory data were separately analyzed (Figs. 1D, 1E). There was no significant difference found between the horizontal and vertical tracking kernel functions, so they were treated equally and averaged in later analysis.

To further quantitatively describe the tracking kernel function, a five-parameter (a, μ, σ_1, σ_2, f) skewed Gabor was fitted to the cross-correlation curve:

$$\text{kernel}(t) = \begin{cases} a \cdot \exp\left(-\frac{(t-\mu)^2}{\sigma_1^2}\right) \cdot \sin\left(2\pi f t\right), & if\ t < \mu \\ a \cdot \exp\left(-\frac{(t-\mu)^2}{\sigma_2^2}\right) \cdot \sin\left(2\pi f t\right), & if\ t \geq \mu \end{cases}, \quad (1)$$

where a and μ represent the peak and the time corresponding the peak, respectively, and σ_1 and σ_2 represent the standard deviation for the left-half and right-half Gaussians, respectively. f together with σ_1 and σ_2 controls the bandwidth of the tracking kernel.

Equation (1) provided a good fit for all participants. The r^2 of all participants and in all three experiments is shown as histograms in Figure D1, Appendix D. The average r^2 in the amblyopic group and normal group was 0.926 ± 0.074 and 0.948 ± 0.053, respectively. The r^2s in the two groups were both greater than 0.9 (both Ps < 0.01).

The peak (the highest point of the curve), latency (the distance between peak and origin), and width (full width at half maximum) of the tracking kernel were derived from the best-fit model (Fig. 1F).

Results

Experiment 1

For each participant, 240 tracking kernels were calculated, and they are sorted according to the target size and shown in each panel of Figure 2. Each kernel is displayed in a single row, with different colors representing different response amplitudes. The mean kernel functions for different target sizes are depicted in Figures 3A and 3B for the amblyopic and normal groups, respectively. The tracking kernel in both amblyopic and normal participants exhibited a similar characteristic pattern. The response reached the maximum value after a short delay of the random walk onset of the target and gradually dropped to baseline. As the target size increased, the kernel responses decreased. At the largest size, some participants showed very poor performance. Visual inspection of Figures 3A and 3B suggests the kernel function of the two groups differed at the smallest target size and became similar at the largest target size.

The parameters of the tracking kernels between the two groups were compared. The peak reflects the system sensitivity to the location change of the target and the tracking accuracy. The latency represents the time at which the response reaches maximum and is equivalent to the response time. Also, the width reflects the sensory and motor noises.[33,51]

The peak of the tracking kernel is plotted as a function of target size for the two groups in Figure 4A, along with the latency in Figure 4B and width in Figure 4C, respectively. Repeated-measures analysis of variance showed that there was a significant effect of target size on the peak ($F(1.649, 46.170) = 200.958$, $P = 4.420 \times 10^{-22}$). The peak decreased as the target size increased. No significant effect of group was found ($F(1, 28) = 2.599$, $P = 0.118$). However, the interaction between group and target size was significant ($F(1.649, 46.170) = 6.205$, $P = 0.007$). At the target size of 11 arcmin, the peak in the amblyopic eye was significantly lower than that in the normal eye (0.089 ± 0.023 [mean ± SD] vs. 0.107 ± 0.020; $t(28) = -2.390$, $P = 0.024$). At the target size of 13 arcmin, the peak in the amblyopic eye was

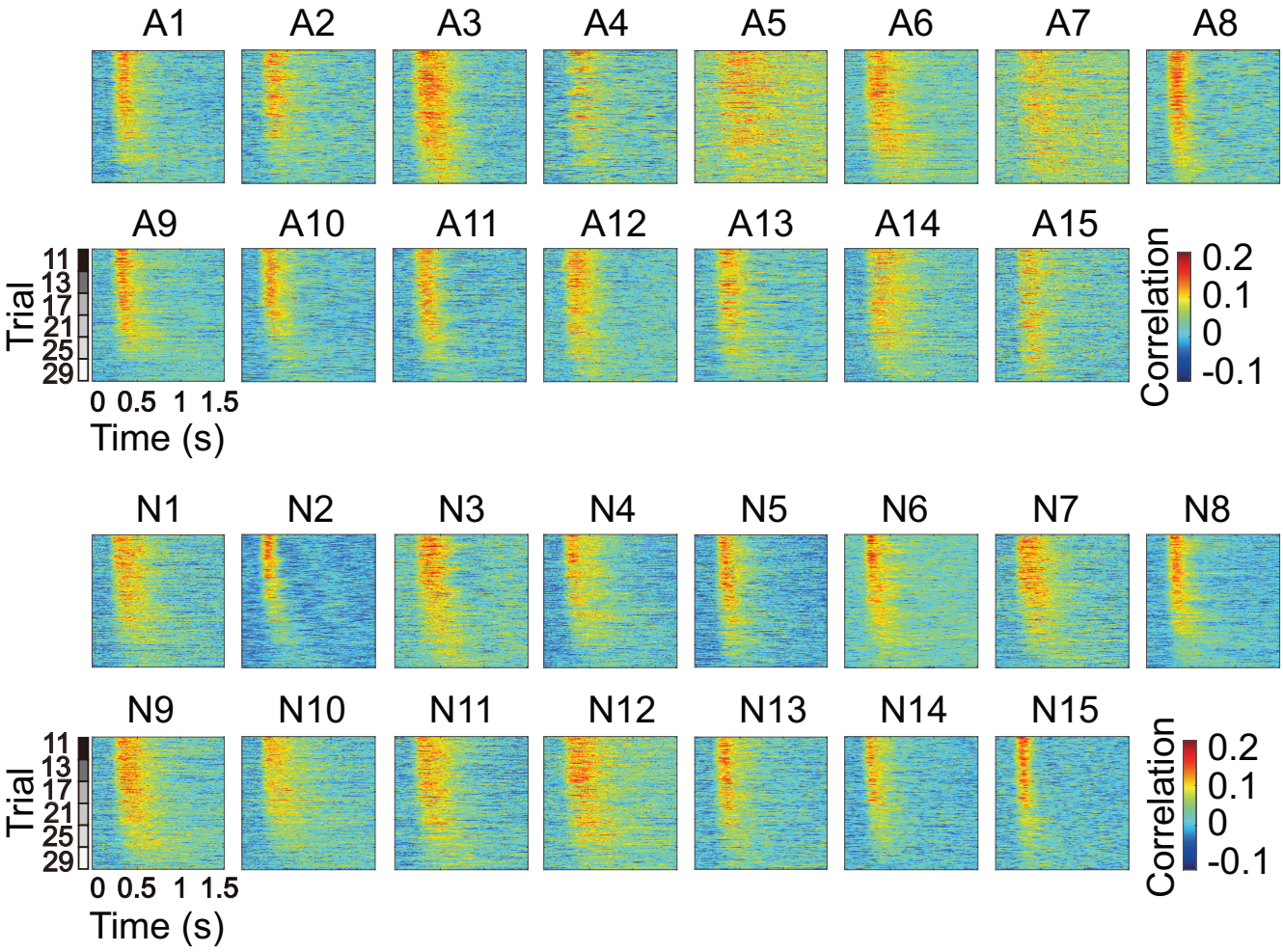

Figure 2. Tracking kernels of the amblyopic (A1–A15) and normal participants (N1–N15). Each tracking kernel is displayed as a row of pixels with color varying along the horizontal axis (time). The kernels in different trials are grouped according to the target size, as indicated by the *gray* label on the left. Horizontal axis represents time.

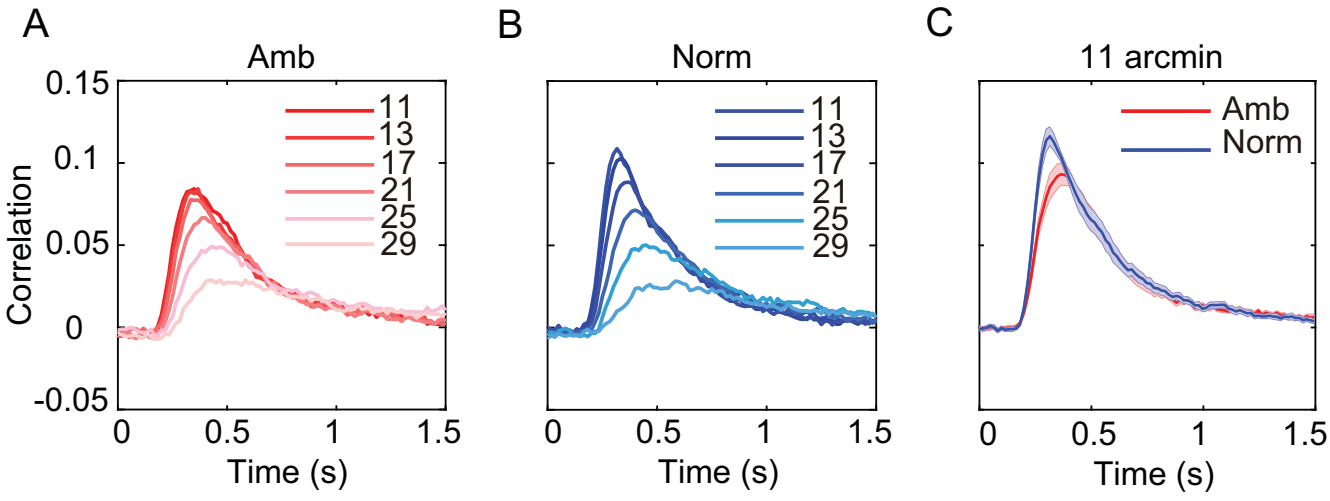

Figure 3. Average tracking kernels of the amblyopic (Amb) and normal groups (Norm) are shown in (**A**) and (**B**), respectively. Different colors correspond to different target sizes. (**C**) The tracking kernel at the target size of 11 arcmin of the amblyopic (*red*) and normal (*blue*) groups. *Shaded areas* represent ±1 standard error. The x-axis represents time, and the y-axis represents the response amplitude/correlation.

Investigative Ophthalmology & Visual Science

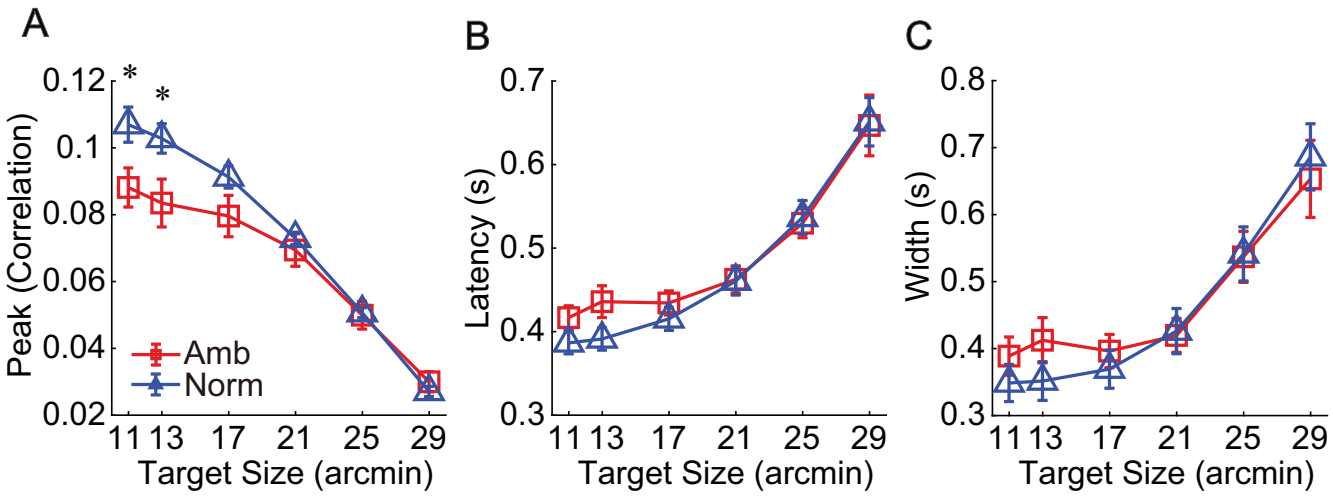

FIGURE 4. The peak (**A**), latency (**B**), and width (**C**) of the tracking kernel are plotted against the target size for the two groups. *Red*: amblyopic eye; *blue*: normal eye. Asterisks represent $P < 0.05$.

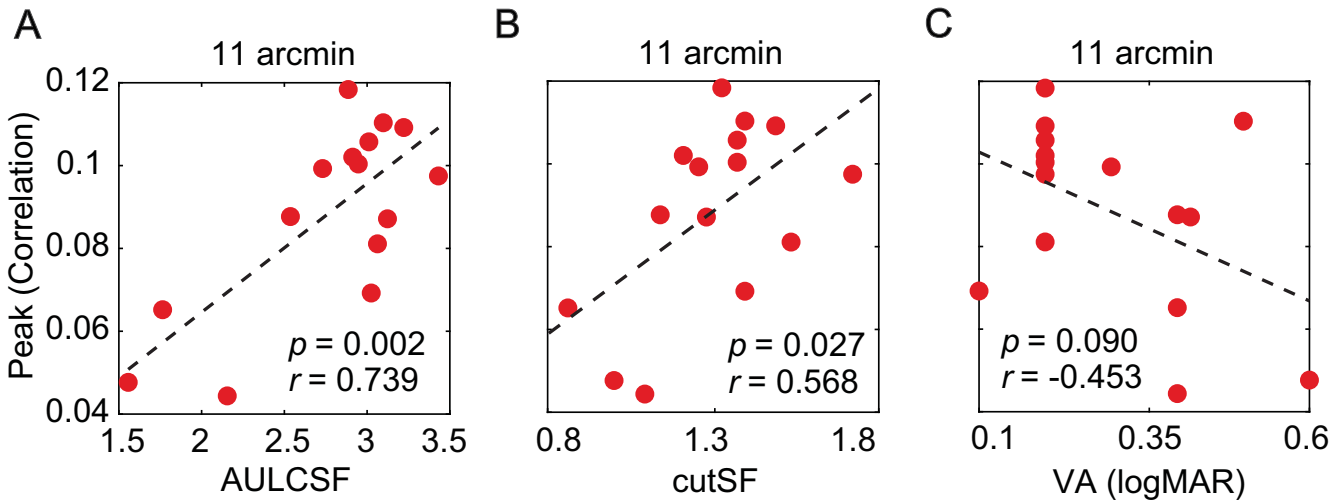

FIGURE 5. The correlation between the peak of the tracking kernel at the target size of 11 arcmin and the AULCSF (**A**), between the peak and cutSF (**B**), and between the peak and VA (**C**) in the amblyopic group.

significantly lower than that in the normal eye (0.084 ± 0.028 vs. 0.103 ± 0.017; $t(23.278) = -2.296$, $P = 0.031$).

The latency increased with the increase in target size ($F(1.232, 34.485) = 107.097$, $P = 4.090 \times 10^{-13}$). The group effect was not significant ($F(1, 28) = 0.397$, $P = 0.534$), nor was the interaction between group and size ($F(1.232, 34.485) = 1.266$, $P = 0.278$). Similarly, the kernel width also increased as the target size got larger ($F(1.393, 38.998) = 54.388$, $P = 2.529 \times 10^{-10}$). No significant effect of group ($F(1, 28) = 0.115$, $P = 0.737$) or the interaction between group and size ($F(1.393, 38.998) = 1.133$, $P = 0.314$) was found. The statistical analyses confirmed our visual inspection in Figures 2 and 3.

The area under the log CSF (AULCSF) and the log cutoff spatial frequency (cutSF) were derived from the CSF for each participant. The AULCSF in the amblyopic eyes was significantly lower than that in the normal eyes (2.764 ± 0.539 vs. 3.115 ± 0.246; $t(28) = -2.293$, $P = 0.030$). Similarly, the cutSF in the amblyopic eyes was lower than that in the normal eyes (1.297 ± 0.217 vs. 1.586 ± 0.143; $t(28) = -4.319$, $P = 1.775 \times 10^{-4}$).

Correlation analyses showed that for the amblyopic eyes, the kernel peak at the target size of 11 arcmin significantly correlated with AULCSF and cutSF (both Ps < 0.05, Figs. 5A, 5B). The correlation between the peak and VA was not significant (Fig. 5C). There was no significant correlation found between the kernel peak and AULCSF or between the kernel peak and cutSF in the normal group (both Ps > 0.05). However, when the data in the two groups were pooled together, the correlations were significant (both Ps < 0.05).

In experiment 1, we found that (1) the tracking performance was modulated by the location uncertainty of target, (2) the tracking performance in the amblyopic eye was worse than that in the normal eye at 11 arcmin as evidenced by the lower peak of the kernel, and (3) the peak correlated with the CSF in the amblyopic group. The next question, then, is whether the tracking performance in the

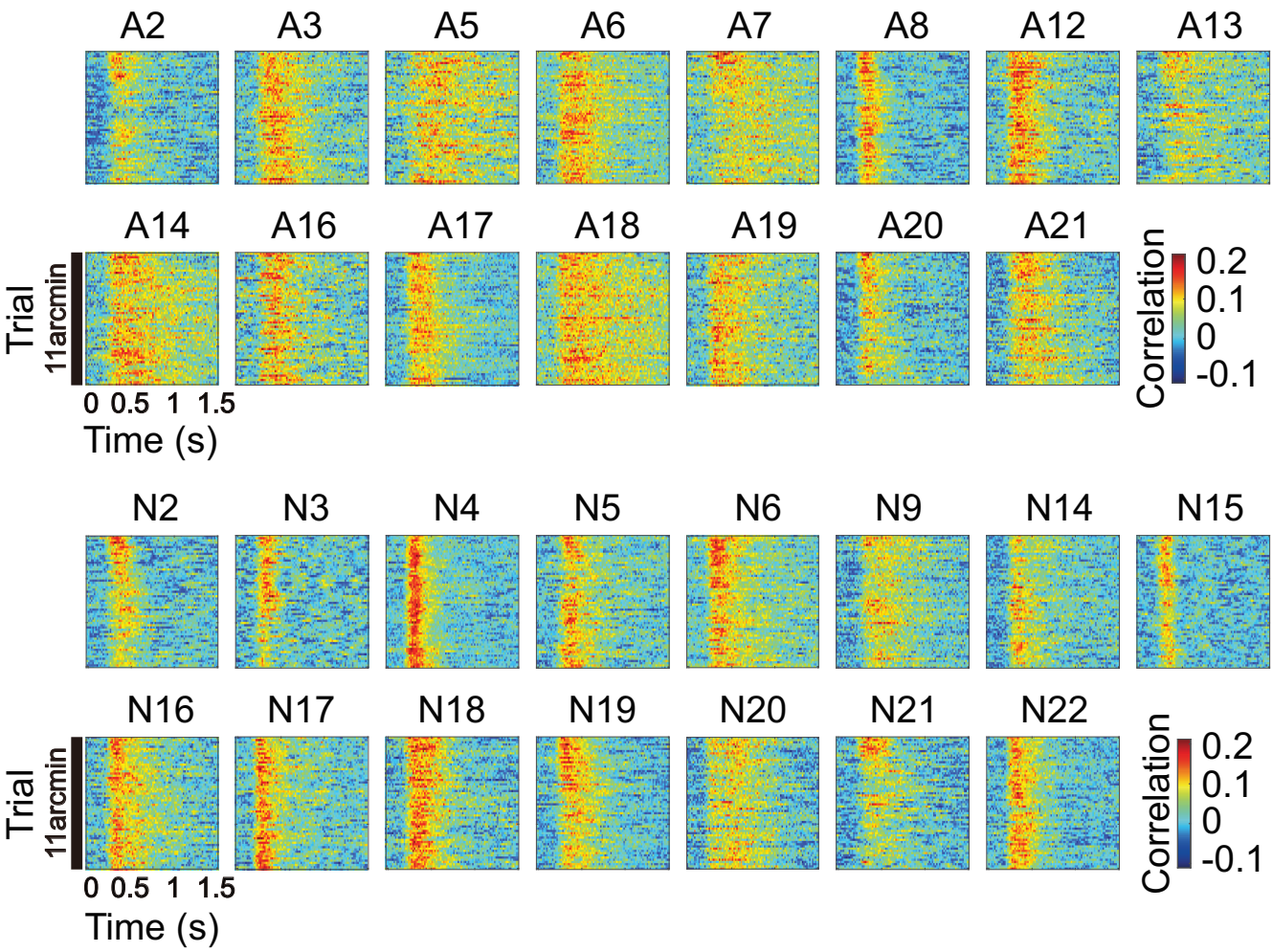

Figure 6. The tracking kernels at the target size of 11 arcmin for each participant in experiment 2. Each tracking kernel is displayed as a row of pixels with color varying along the horizontal axis (time).

amblyopic eye is still worse than that in the normal eye, when the visual input is equalized at individual's threshold level.

Experiment 2

The motion detection threshold of the amblyopic and normal groups was 0.217 ± 0.092 and 0.158 ± 0.052, respectively. The threshold in the amblyopic group was significantly higher than that in the normal group ($t(28) = 2.193$, $P = 0.037$). The tracking kernels of each participant are shown in each panel of Figure 6, and the mean kernel function in the amblyopic and normal groups is plotted in Figure 7A. The peak in the amblyopic group was found significantly lower than that in the normal group (0.070 ± 0.019 vs. 0.087 ± 0.019, $t(28) = -2.425$, $P = 0.022$, Fig. 7B). Compared to that in the normal group, the tracking kernel in the amblyopic group also showed a longer latency (0.507 ± 0.083 vs. 0.432 ± 0.073, $t(28) = 2.647$, $P = 0.013$, Fig. 7C) and broader width (0.552 ± 0.159 vs. 0.412 ± 0.144, $t(28) = 2.540$, $P = 0.017$, Fig. 7D). In addition, no correlation between the kernel peak and AULCSF, cutSF, or VA was found, suggesting that the visibility of the target was well controlled as intended (Fig. 8).

The result in experiment 2 indicates that the tracking performance in the amblyopic eye remained impaired, even when the visual input was equalized to individual's threshold level.

Experiment 3

In experiment 3, the participants were asked to track the target at the individual's threshold for a 500-ms random walk motion. The motion detection threshold of the amblyopic and normal groups was 0.115 ± 0.046 and 0.106 ± 0.037, respectively. The threshold of a 500-ms duration in amblyopic patients was significantly lower than that of 150 ms (0.115 ± 0.046 vs. 0.268 ± 0.110, $t(6) = -3.692$, $P = 0.010$) found in experiment 2. There was no difference in the threshold found between two groups ($t(12) = 0.387$, $P = 0.705$).

The tracking kernels of each participant are shown in each panel of Figure 9, and the mean kernel function in the amblyopic and normal groups is plotted in Figure 10A. The peak in the amblyopic group was found significantly lower than that in the normal group (0.061 ± 0.022 vs. 0.098 ± 0.015, $t(12) = -3.687$, $P = 0.003$, Fig. 10B). Compared to that in the normal groups, the tracking kernel in the amblyopic

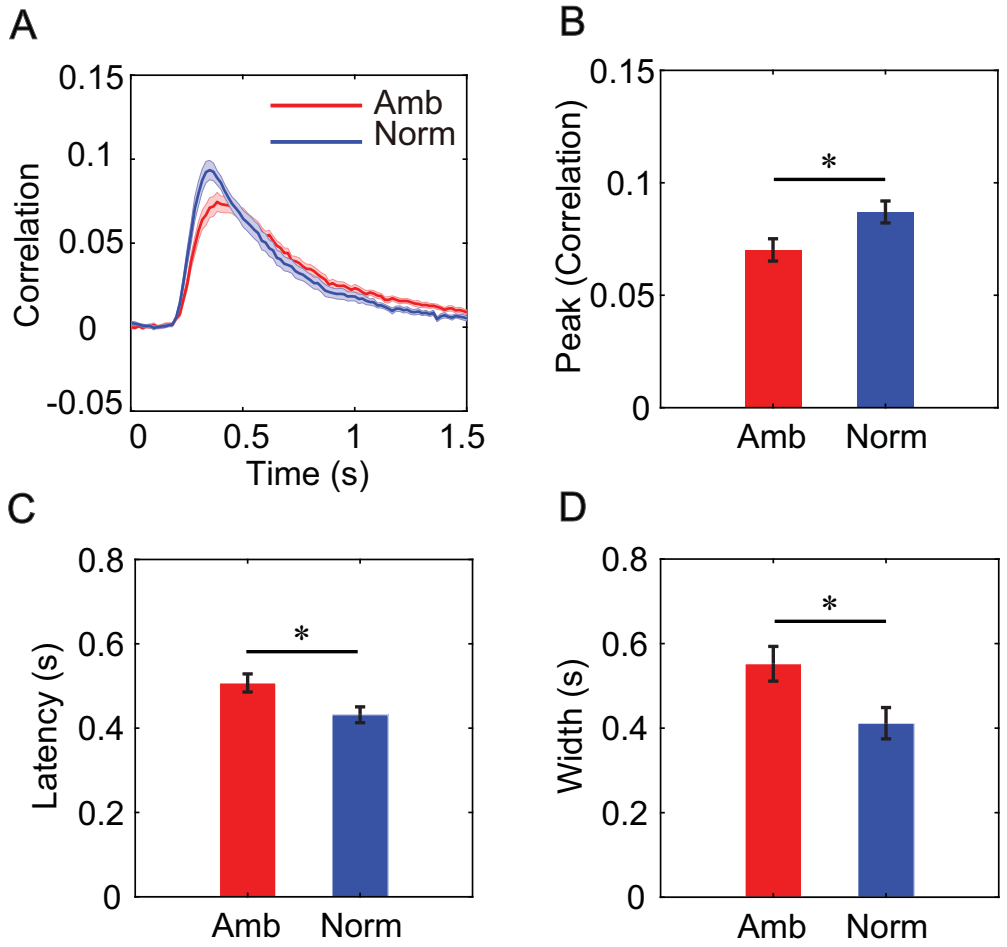

Figure 7. (**A**) Average tracking kernel at the target size of 11 arcmin for the amblyopic and normal groups. *Shaded areas* represent ±1 standard error. The peaks (**B**), latencies (**C**), and widths (**D**) of the kernels in the two groups are compared. *Red* and *blue* represent the amblyopic and normal groups, respectively. *Error bars* indicate ±1 standard error. *$P < 0.05$.

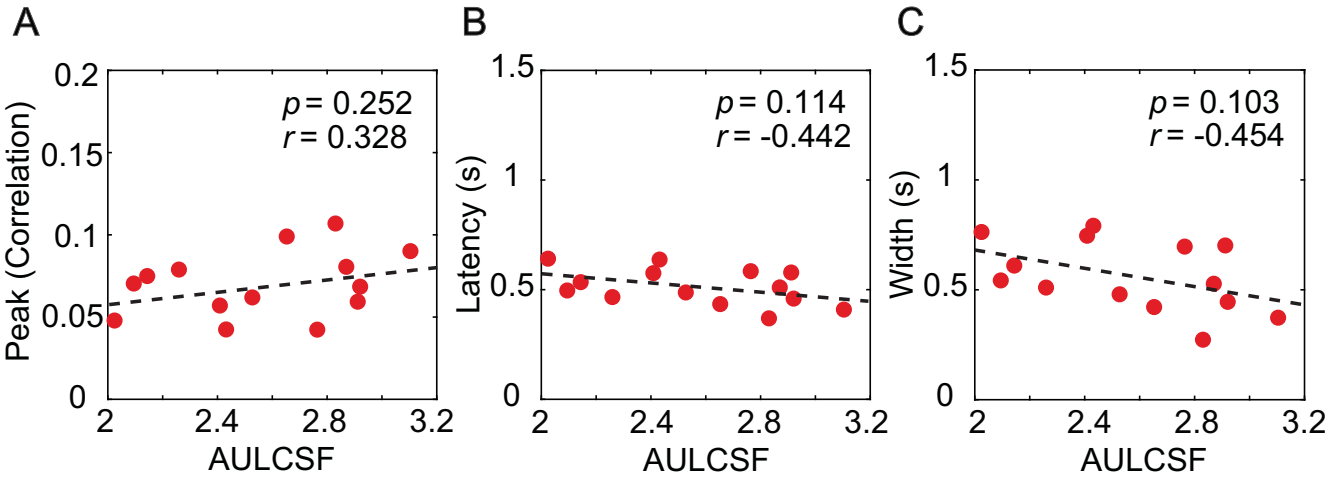

Figure 8. The correlation between the peak of the tracking kernel and AULCSF (**A**), the latency of tracking kernel and AULCSF (**B**), and the width and AULCSF (**C**) in the amblyopic group. No significant correlation was found.

group also showed a longer latency (0.551 ± 0.128 vs. 0.394 ± 0.048, $t(12) = 3.032$, $P = 0.010$, Fig. 10C) and broader width (0.584 ± 0.190 vs. 0.320 ± 0.080, $t(12) = 3.388$, $P = 0.005$, Fig. 10D). In addition, no significant correlation between the tracking kernels and AULCSF was found, again suggesting that the visibility of the target was well controlled as intended (Fig. 11). The result of experiment 3 was exactly the same as that of experiment 2.

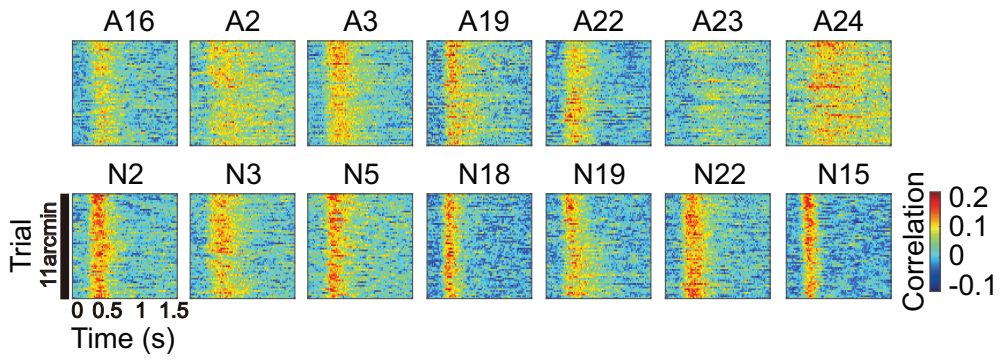

Figure 9. The tracking kernels at the target size of 11 arcmin for each participant in experiment 3.

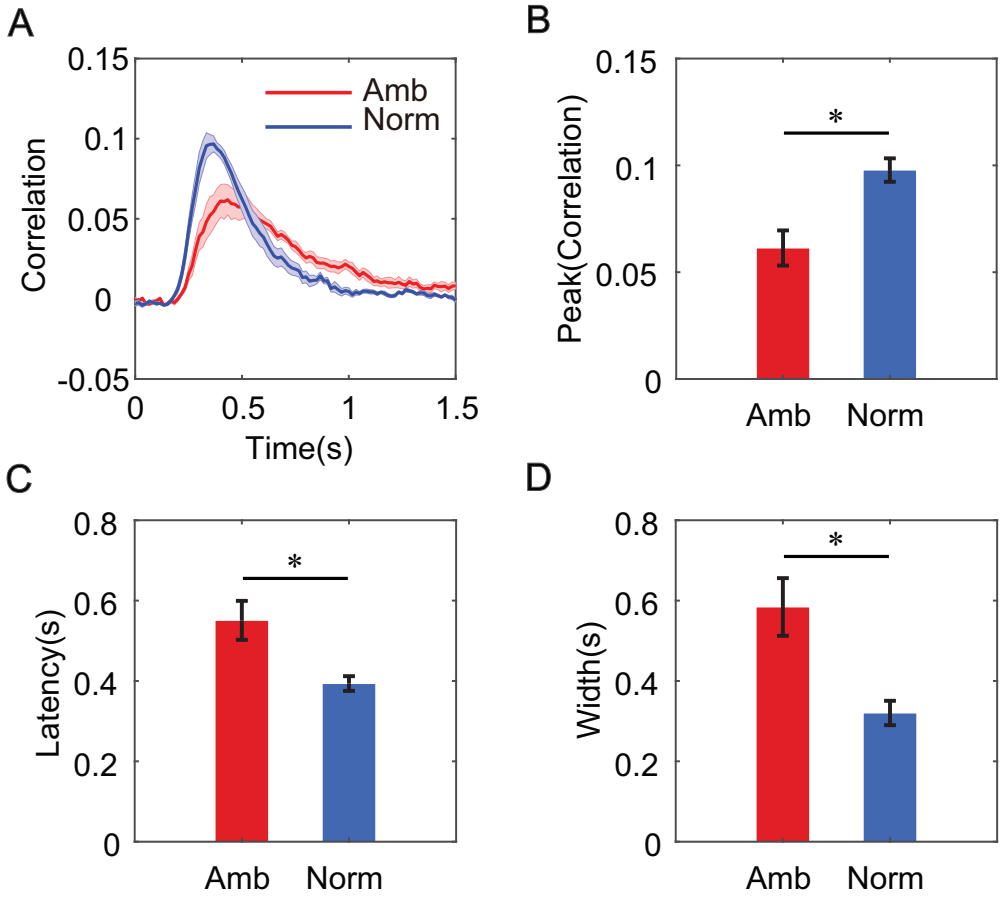

Figure 10. (**A**) Average tracking kernels at the target size of 11 arcmin for the amblyopic and normal groups. *Shaded areas* represent ±1 standard error. The peaks (**B**), latencies (**C**), and widths (**D**) of the kernels in the two groups are compared. *Red* and *blue* represent the amblyopic and normal groups, respectively. *Error bars* indicate ±1 standard error. *$P < 0.05$.

Discussion

In this study, by adopting a continuous tracking paradigm[24–27] and systematically manipulating visual input, we investigated whether the observed visuomotor deficit in amblyopia was due to the impaired vision only or might also involve other deficits. Participants were instructed to continuously track a randomly walking Gaussian target with a computer mouse. In experiment 1, the tracking performance of both amblyopic and normal participants was measured at six different target sizes. After showing the validity of the continuous tracking paradigm, we further measured the tracking performance at an individual's threshold level for the two groups in experiment 2 and experiment 3.

The Continuous Tracking Paradigm

The conventional psychophysical experiment has discrete trials with a well-separated trial structure (i.e., stimulus

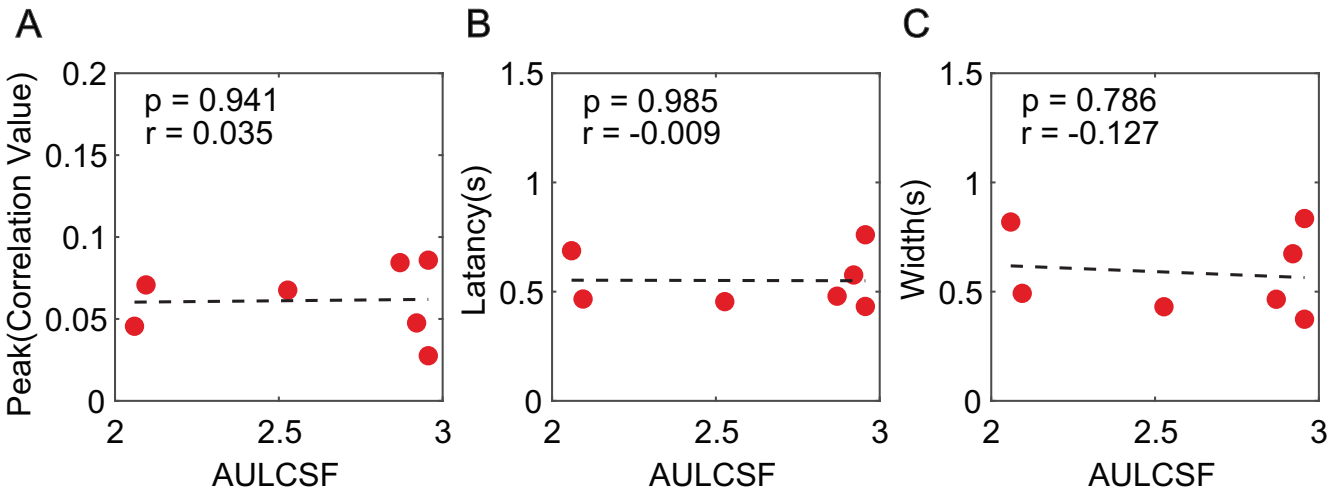

Figure 11. The correlation between the peak and AULCSF (**A**), the latency and AULCSF (**B**), and the width and AULCSF (**C**) of the tracking kernel in the amblyopic group. No significant correlation was found.

presentation phase and response collection phase). It typically collects one response in a trial and needs hundreds or thousands of trials to evaluate the human performance (the percentage correct or d'). In contrast, the continuous tracking paradigm has a long stream of dynamic stimuli with simultaneous response collection and thus is capable of collecting multiple responses within a second.[24–27,33,50] It has been shown that the continuous tracking paradigm can provide the psychophysical measure equivalent to that in a conventional trial-based paradigm[24,26] with similar precision but in a shorter time (120 tracking trials vs. 4860 discrete trials).[24] In addition, the continuous tracking task is more natural compared to the repetitive conventional trials because our daily visual tasks such as driving or looking for a familiar face in the crowded street are rarely discrete. Instead, human perception and behavior involve continuous integration and synthesis of visual input, sensory processing, cognitive decision, and motor execution over time.[25,52]

The high-throughput stimulus–response data series generated by the continuous tracking paradigm allowed us to apply cross-correlation to study human tracking in a more rigorous manner.[24,25,33,53] Cross-correlation has been widely used in the analysis of neural data to reveal the neuron receptive fields in physiology.[28,30–32] It has also been employed to uncover the spatiotemporal weighting functions of sensory processes in psychophysics, such as orientation tuning,[33,54] disparity tuning,[55] perceptual template,[56,57] eye movement,[50] and face recognition.[51,58] Compared with conventional psychophysical measures, the results from the continuous tracking paradigm have more detailed dynamics across the space/feature/time domain. We characterized the tracking performance by the tracking kernel, calculated as the cross-correlation between the target and mouse displacements. The kernel function represents how the system is influenced by preceding dynamic sensory stimuli, or how the observer responds to the previous target displacement at each time point. With the tracking kernel, we quantified the tracking performance for both amblyopic and normal participants with three parameters: the peak, latency, and width. The continuous tracking paradigm with the cross-correlation analysis provides a very convenient and powerful tool to study human behavior and underlying mechanisms, especially in clinical populations.

The Tracking Deficits in Amblyopia

During tracking, the observer performance was determined by the ratio between the internal representations of the step size (0° ± 0.02°) of the random walk and the uncertainty of target location, similar to how signal-to-noise ratio (d') affects performance in signal detection theory (see Fig. B2, Appendix B). In experiment 1, we measured the tracking performance with different uncertainty of target location. This design is very similar to the external noise paradigm, which measures an observer's threshold at different external noise levels.[59] The characteristics of the threshold versus external noise contrast function are well established. When the external noise is low, the observer threshold is determined by the internal noise of the observer, while when the external noise is high, the threshold is determined by the external noise.[60–62]

At the smallest target size with the lowest location uncertainty, the tracking performance depended on the internal noise of the visual system. Because the amblyopic visual system was known to have greater internal noise[60,61] or larger spatial uncertainty[63,64] than the normal visual system, the tracking performance of the amblyopic participants was poorer than that of normal observers at the smallest target size (uncertainty). At large target size, the visual system was dominated by the external location uncertainty, which was the same level for both groups, so the amblyopic and normal observers showed comparable performance at the largest target size.

The tracking performance in the amblyopic group was highly correlated with their spatial contrast sensitivity function, especially at a high spatial frequency. Tracking the small step size (0° ± 0.02°) of the random walk would involve high-frequency channels. It has been reported that the internal noise increases with the spatial frequency,[65] and the increase is even greater in the amblyopic visual system compared to the normal visual system.[61] Together, the tracking kernel, estimated using the continuous tracking paradigm, effectively captured both the external uncertainty

of the visual input and the internal uncertainty of the visual system. These findings confirm that the continuous tracking paradigm is a valid tool for evaluating visual tracking performance.

By analyzing the hand movement recorded with an infrared camera, people have found that amblyopic children and adults exhibit prolonged movement execution time and a higher error rate when grasping objects in the real world.[17,19,66] Melmoth et al.[66] also found a significant correlation between the grip application time and stereoacuity, suggesting that the visuomotor deficits in amblyopia arise from dysfunction of dorsal stream areas involved in processing disparity information.[67–69] In our study, both amblyopic and normal participants tracked a two-dimensional target moving in the frontoparallel plane monocularly. At the smallest target size, the tracking performance in the amblyopic eye highly correlated with the AULCSF as well as the cutoff frequency. It indicates that the tracking deficits in amblyopia are related to the impairment of sensitivity loss in the amblyopic eye, especially at high spatial frequencies. The results in experiment 1 extend previous findings and suggest that visual processing impairments, not just abnormal stereopsis, contribute to the observed deterioration in tracking performance for the amblyopic eye.

It has been reported that the temporal integration of the human visual system for motion detection is over about 100 ms[44–47] and is longer when the stimulus speed is slower (up to 200 ms at 0.5 deg/s).[45,46] We thus chose 150 ms for the duration of the minimovie in experiment 2. However, these results were based on normal people. There was a mixed report on motion integration in amblyopia.[15,70,71] It is possible that 150 ms is not a good choice for amblyopia. Moreover, the 150-ms duration was shorter than the saccade latency[72] and did not allow eye movement. In contrast, the observer was allowed to move their eye to follow the target during tracking. To address the mismatch in eye movement between the 2IFC motion detection and tracking, we used a 500-ms random walk stimulus In experiment 3. The stimulus with a longer duration in the 2IFC task was more similar to that in the tracking task, which enabled the observer to freely follow the moving target. The results were the same as those in experiment 2.

Experiments 2 and 3 revealed that even when stimulus visibility was equated, amblyopic participants still displayed significantly poorer tracking performance. Notably, no significant correlation existed between the CSF and the kernel peak. There must be other deficits that contributed to the poorer tracking performance in amblyopia.

It has been reported that the amblyopic visual system is associated with an increased level of equivalent intrinsic blur,[73,74] which could result in elevated spatial resolution or location uncertainty. Moreover, studies have shown that even when stimulus visibility was accounted for, the spatial uncertainty was greater in amblyopic eyes than nonamblyopic eyes, or normal eyes for targets.[63,73,74] Therefore, it is possible that the greater intrinsic blur in the amblyopic visual system[74,75] affected the observed tracking performance in our study.

On the other hand, Hess and Holliday[11] found that the spatial localization deficits in the anisometropic amblyopes (as were most of our amblyopic participants) can be explained by the contrast sensitivity deficit. In this case, deficits in brain areas beyond the visual cortex could play a role in the impaired tracking in amblyopia.

Besides visual perception, the visuomotor control involves other essential and complex processes,[76] including automatic programming for the timing and metrics of the movements of the skilled implementation, monitoring, and online correction of movement for precise control. A motor plan is generated prior to the onset of movement based on the intrinsic property (i.e., size, mass) of the target gathered from vision or other sensory modalities. Our finding suggests that an additional deficit, likely located downstream of the visual cortex, contributes to the impaired tracking performance observed in amblyopia. This aligns with previous findings by Niechwiej-Szwedo et al.,[77] who demonstrated that amblyopic patients exhibited significantly poorer performance in reaching movements compared to normal participants with artificially induced monocular blur and concluded that the decreased visual tracking performance in amblyopic patients cannot be solely attributed to a loss of visual acuity. Additional studies on reaction time in amblyopic patients[78,79] also suggest the presence of a postsensory delay in visual tasks, possibly originating from higher-level brain regions affected by amblyopia. The intraparietal and parietofrontal networks are believed to receive the information from the visual cortex and transform it into the action commands.[80] The tracking deficit observed in experiments 2 and 3 could be a result of the disturbed assembly of motion plans in individuals with amblyopia.

An ongoing motor plan is also updated continuously by integrating the sensory inflow and the motor outflow to evaluate the consequences of the motor commands for precise movement control. In our experiment, the observer was required to keep monitoring the subtle displacement of the target and moving the mouse to minimize the distance between the target's location and the cursor. The tracking deficit found in experiments 2 and 3 might also reflect the impaired online control in the amblyopic visual system. Niechwiej-Szwedo et al.[19] speculated that an amblyopic patient's ability to engage in online control is impaired, making it less effective in correcting the potential trajectory errors, because they observed that the participants with amblyopia exhibited a different strategy in grasping with a lower peak acceleration. The posterior parietal cortex (PPC) is essential in the sensorimotor transformations and online control that underlie visually guided reaching.[21,81–83] Resting state magnetic resonance imaging studies found abnormal spontaneous activity in PPC in amblyopic patients.[84,85] Thus, experiments 2 and 3 suggest that the deficits in the PPC may contribute to their impaired tracking performance.

In conclusion, we found that the tracking performance was significantly poorer in the amblyopic participants than in normal people, even when the stimulus visibility was equated for the two groups. The result suggested that besides contrast sensitivity deficits, other deficits contributed to the decreased tracking performance in amblyopia. Our study also demonstrated that the continuous tracking paradigm could provide a useful tool for investigating the tracking performance in clinical populations.

Acknowledgments

The authors thank the editorial board member and the two anonymous reviewers for their helpful comments that improved the quality of the manuscript.

Supported by the National Key R&D Program of China (2023YFC3604101 to FH), the National Science and Tech-

nology Innovation 2030 Major Program (2022ZD0204801 to FH), and the National Natural Science Foundation of China (NSFC82371097 to FH).

Disclosure: **C. Li**, None; **Y. Yang**, None; **J. Zhu**, None; **Y. Han**, None; **J. He**, None; **J. Wang**, None; **Y. Feng**, None; **J. Yuan**, None; **X. Huang**, None; **R. Liu**, None; **H. Zhang**, None; **X. Ruan**, None; **F. Hou**, None

References

1. DeSantis D. Amblyopia. *Pediatr Clin*. 2014;61:505–518.
2. Webber AL, Wood J. Amblyopia: prevalence, natural history, functional effects and treatment. *Clin Exp Optom*. 2005;88:365–375.
3. Kiorpes L. Understanding the development of amblyopia using macaque monkey models. *Proc Natl Acad Sci*. 2019;116:26217–26223.
4. McKee SP, Levi DM, Movshon JA. The pattern of visual deficits in amblyopia. *J Vis*. 2003;3:5.
5. Kiorpes L, Kiper DC, O'keefe LP, Cavanaugh JR, Movshon JA. Neuronal correlates of amblyopia in the visual cortex of macaque monkeys with experimental strabismus and anisometropia. *J Neurosci*. 1998;18:6411–6424.
6. Hess R, Howell E. The threshold contrast sensitivity function in strabismic amblyopia: evidence for a two type classification. *Vis Res*. 1977;17:1049–1055.
7. Zele AJ, Pokorny J, Lee DY, Ireland D. Anisometropic amblyopia: spatial contrast sensitivity deficits in inferred magnocellular and parvocellular vision. *Invest Ophthalmol Vis Sci*. 2007;48:3622–3631.
8. Pang Y, Allen M, Robinson J, Frantz KA. Contrast sensitivity of amblyopic eyes in children with myopic anisometropia. *Clin Exp Optom*. 2019;102:57–62.
9. Levi D, Harwerth RS. Spatio-temporal interactions in anisometropic and strabismic amblyopia. *Invest Ophthalmol Vis Sci*. 1977;16:90–95.
10. Volkers A, Hagemans K, Van Der Wildt G, Schmitz P. Spatial contrast sensitivity and the diagnosis of amblyopia. *Br J Ophthalmol*. 1987;71:58–65.
11. Hess RF, Holliday IE. The spatial localization deficit in amblyopia. *Vis Res*. 1992;32:1319–1339.
12. Giaschi D, Lo R, Narasimhan S, Lyons C, Wilcox LM. Sparing of coarse stereopsis in stereodeficient children with a history of amblyopia. *J Vis*. 2013;13:17.
13. Levi DM, Knill DC, Bavelier D. Stereopsis and amblyopia: a mini-review. *Vis Res*. 2015;114:17–30.
14. Simmers A, Ledgeway T, Mansouri B, Hutchinson C, Hess R. The extent of the dorsal extra-striate deficit in amblyopia. *Vis Res*. 2006;46:2571–2580.
15. Simmers AJ, Ledgeway T, Hess RF, McGraw PV. Deficits to global motion processing in human amblyopia. *Vis Res*. 2003;43:729–738.
16. Grant S, Moseley MJ. Amblyopia and real-world visuomotor tasks. *Strabismus*. 2011;19:119–128.
17. Suttle CM, Melmoth DR, Finlay AL, Sloper JJ, Grant S. Eye-hand coordination skills in children with and without amblyopia. *Invest Ophthalmol Vis Sci*. 2011;52:1851–1864.
18. Grant S, Melmoth DR, Morgan MJ, Finlay AL. Prehension deficits in amblyopia. *Invest Ophthalmol Vis Sci*. 2007;48:1139–1148.
19. Niechwiej-Szwedo E, Goltz HC, Chandrakumar M, Wong AMF. Effects of strabismic amblyopia on visuomotor behavior: Part II. Visually guided reaching. *Invest Ophthalmol Vis Sci*. 2014;55:3857–3865.
20. Niechwiej-Szwedo E, Goltz HC, Chandrakumar M, Wong AM. Effects of strabismic amblyopia and strabismus without amblyopia on visuomotor behavior: III. Temporal eye–hand coordination during reaching. *Invest Ophthalmol Vis Sci*. 2014;55:7831–7838.
21. Eskandar EN, Assad JA. Dissociation of visual, motor and predictive signals in parietal cortex during visual guidance. *Nat Neurosci*. 1999;2:88–93.
22. Archambault PS, Ferrari-Toniolo S, Caminiti R, Battaglia-Mayer A. Visually-guided correction of hand reaching movements: the neurophysiological bases in the cerebral cortex. *Vis Res*. 2015;110:244–256.
23. Castiello U. The neuroscience of grasping. *Nat Rev Neurosci*. 2005;6:726–736.
24. Bonnen K, Burge J, Yates J, Pillow J, Cormack LK. Continuous psychophysics: target-tracking to measure visual sensitivity. *J Vis*. 2015;15:14.
25. Huk A, Bonnen K, He BJ. Beyond trial-based paradigms: continuous behavior, ongoing neural activity, and natural stimuli. *J Neurosci*. 2018;38:7551–7558.
26. Ambrosi P, Burr DC, Cicchini GM. Ideal observer analysis for continuous tracking experiments. *J Vis*. 2022;22:3.
27. Bhat A, Cicchini GM, Burr DC. Inhibitory surrounds of motion mechanisms revealed by continuous tracking. *J Vis*. 2018;18:7.
28. Ringach D, Shapley R. Reverse correlation in neurophysiology. *Cogn Sci*. 2004;28:147–166.
29. Nykamp DQ, Ringach DL. Full identification of a linear-nonlinear system via cross-correlation analysis. *J Vis*. 2002;2:1–11.
30. Ringach DL, Hawken MJ, Shapley R. Dynamics of orientation tuning in macaque primary visual cortex. *Nature*. 1997;387:281–284.
31. Ringach DL, Hawken MJ, Shapley R. Dynamics of orientation tuning in macaque V1: the role of global and tuned suppression. *J Neurophysiol*. 2003;90:342–352.
32. Kovacic G, Tao L, Cai D, Shelley MJ. Theoretical analysis of reverse-time correlation for idealized orientation tuning dynamics. *J Comput Neurosci*. 2008;25:401–438.
33. Zhu J, Ruan X, Li C, et al. Psychophysical reverse correlation revealed broader orientation tuning and prolonged reaction time in amblyopia. *Invest Ophthalmol Vis Sci*. 2022;63:3–3.
34. Ho R, Thompson B, Babu RJ, Dalton K. Sighting ocular dominance magnitude varies with test distance. *Clin Exp Optom*. 2018;101:276–280.
35. Gregori NZ, Feuer W, Rosenfeld PJ. Novel method for analyzing Snellen visual acuity measurements. *Retina*. 2010;30:1046–1050.
36. Chaikitmongkol V, Nanegrungsunk O, Patikulsila D, Ruamviboonsuk P, Bressler NM. Repeatability and agreement of visual acuity using the ETDRS number chart, Landolt C chart, or ETDRS alphabet chart in eyes with or without sight-threatening diseases. *JAMA Ophthalmol*. 2018;136:286–290.
37. Zhao L, Wu H. The effect of dot size in random-dot stereograms on the results of stereoacuity measurements. *BMC Ophthalmol*. 2020;20:1–6.
38. Hou F, Huang C-B, Lesmes L, et al. qCSF in clinical application: efficient characterization and classification of contrast sensitivity functions in amblyopia. *Invest Ophthalmol Vis Sci*. 2010;51:5365–5377.
39. Zheng H, Shen M, He X, et al. Comparing spatial contrast sensitivity functions measured with digit and grating stimuli. *Transl Vis Sci Technol*. 2019;8:16.
40. Lesmes LA, Lu ZL, Baek J, Albright TD. Bayesian adaptive estimation of the contrast sensitivity function: the quick CSF method. *J Vis*. 2010;10:17.1–17.21.
41. Kleiner M, Brainard D, Pelli D. What's new in psychtoolbox-3? *Perception*. 2007;36:1–16.
42. Elze T, Tanner TG. Temporal properties of liquid crystal displays: implications for vision science experiments. *PLOS ONE*. 2012;7:e44048.

Investigative Ophthalmology & Visual Science

43. Hallum LE, Cloherty SL. Liquid-crystal display (LCD) of achromatic, mean-modulated flicker in clinical assessment and experimental studies of visual systems. *PLoS One*. 2021;16:e0248180.
44. Geisler WS. Motion streaks provide a spatial code for motion direction. *Nature*. 1999;400:65–69.
45. Snowden RJ, Braddick OJ. The temporal integration and resolution of velocity signals. *Vis Res*. 1991;31:907–914.
46. Burr DC. Temporal summation of moving images by the human visual system. *Proc R Soc London Ser B Biol Sci*. 1981;211:321–339.
47. Burr DC, Santoro L. Temporal integration of optic flow, measured by contrast and coherence thresholds. *Vis Res*. 2001;41:1891–1899.
48. Chung STL, Kumar G, Li RW, Levi DM. Characteristics of fixational eye movements in amblyopia: limitations on fixation stability and acuity? *Vis Res*. 2015;114:87–99.
49. Levitt H. Transformed up-down methods in psychoacoustics. *J Acoustical Soc Am*. 1971;49:467–477.
50. Mulligan JB, Stevenson SB, Cormack LK. (2013). Reflexive and voluntary control of smooth eye movements. In Rogowitz BE, Pappas TN, de Ridder H, eds. *Proceedings of SPIE, Human Vision and Electronic Imaging XVIII: Vol. 8651* (pp. 1–22).
51. Okazawa G, Sha L, Purcell BA, Kiani R. Psychophysical reverse correlation reflects both sensory and decision-making processes. *Nat Commun*. 2018;9:3479.
52. He BJ, Zempel JM, Snyder AZ, Raichle ME. The temporal structures and functional significance of scale-free brain activity. *Neuron*. 2010;66:353–369.
53. Bonnen K, Huk AC, Cormack LK. Dynamic mechanisms of visually guided 3D motion tracking. *J Neurophysiol*. 2017;118:1515–1531.
54. Ringach DL. Tuning of orientation detectors in human vision. *Vis Res*. 1998;38:963–972.
55. Neri P, Parker AJ, Blakemore C. Probing the human stereoscopic system with reverse correlation. *Nature*. 1999;401:695–698.
56. Kuai S-G, Levi D, Kourtzi Z. Learning optimizes decision templates in the human visual cortex. *Curr Biol*. 2013;23:1799–1804.
57. Neri P, Heeger DJ. Spatiotemporal mechanisms for detecting and identifying image features in human vision. *Nat Neurosci*. 2002;5:812–816.
58. Gouki O, Long S, Roozbeh K. Linear integration of sensory evidence over space and time underlies face categorization. *J Neurosci*. 2021;41:7876.
59. Lu Z-L, Dosher BA. Characterizing human perceptual inefficiencies with equivalent internal noise. *J Opt Soc Am A*. 1999;16:764–778.
60. Huang C, Tao L, Zhou Y, Lu ZL. Treated amblyopes remain deficient in spatial vision: a contrast sensitivity and external noise study. *Vis Res*. 2007;47:22–34.
61. Xu P, Lu ZL, Qiu Z, Zhou Y. Identify mechanisms of amblyopia in Gabor orientation identification with external noise. *Vis Res*. 2006;46:3748–3760.
62. Pelli DG. The quantum efficiency of vision. In Blakemore C, ed. *Vision: coding and efficiency*. New York: Cambridge University Press; 1990:3–24.
63. Wang H, Levi DM, Klein SA. Spatial uncertainty and sampling efficiency in amblyopic position acuity. *Vis Res*. 1998;38:1239–1251.
64. Levi DM, Klein SA. Noise provides some new signals about the spatial vision of amblyopes. *J Neurosci*. 2003;23:2522–2526.
65. Hou F, Lu Z-L, Huang C-B. The external noise normalized gain profile of spatial vision. *J Vis*. 2014;14:9.
66. Melmoth DR, Finlay AL, Morgan MJ, Grant S. Grasping deficits and adaptations in adults with stereo vision losses. *Invest Ophthalmol Vis Sci*. 2009;50:3711–3720.
67. Mendola JD, Conner IP, Roy A, et al. Voxel-based analysis of MRI detects abnormal visual cortex in children and adults with amblyopia. *Hum Brain Mapp*. 2005;25:222–236.
68. Backus BT, Fleet DJ, Parker AJ, Heeger DJ. Human cortical activity correlates with stereoscopic depth perception. *J Neurophysiol*. 2001;86:2054–2068.
69. Tsao DY, Vanduffel W, Sasaki Y, et al. Stereopsis activates V3A and caudal intraparietal areas in macaques and humans. *Neuron*. 2003;39:555–568.
70. Hess RF, Mansouri B, Dakin SC, Allen HA. Integration of local motion is normal in amblyopia. *J Opt Soc Am A Opt Image Sci Vis*. 2006;23:986–992.
71. Yasmine E-S, Lynne K, Adam K, Movshon JA. Visual motion processing by neurons in area MT of macaque monkeys with experimental amblyopia. *J Neurosci*. 2010;30:12198.
72. Yang Q, Bucci MP, Kapoula Z. The latency of saccades, vergence, and combined eye movements in children and in adults. *Invest Ophthalmol Vis Sci*. 2002;43:2939–2949.
73. Barbeito R, Bedell HE, Flom MC. Does impaired contrast sensitivity explain the spatial uncertainty of amblyopes? *Invest Ophthalmol Vis Sci*. 1988;29:323–326.
74. Levi DM, Klein SA. Equivalent intrinsic blur in amblyopia. *Vis Res*. 1990;30:1995–2022.
75. Abbas Farishta R, Yang CL, Farivar R. Blur representation in the amblyopic visual system using natural and synthetic images. *Invest Ophthalmol Vis Sci*. 2022;63:3.
76. Milner AD, Goodale MA. Two visual systems re-viewed. *Neuropsychologia*. 2008;46:774–785.
77. Niechwiej-Szwedo E, Kennedy SA, Colpa L, Chandrakumar M, Goltz HC, Wong AMF. Effects of induced monocular blur versus anisometropic amblyopia on saccades, reaching, and eye-hand coordination. *Invest Ophthalmol Vis Sci*. 2012;53:4354–4362.
78. Ruan X, Lin L, Ying X, et al. Decomposing the response time in amblyopia: a drift diffusion model analysis. *Invest Ophthalmol Vis Sci*. 2023;64:25.
79. Farzin F, Norcia AM. Impaired visual decision-making in individuals with amblyopia. *J Vis*. 2011;11:6–6.
80. Battaglia-Mayer A, Caminiti R. Parieto-frontal networks for eye–hand coordination and movements. In: Vallar G, Coslett HB, eds. *Handb Clin Neurol*. Amsterdam: Elsevier; 2018:499–524.
81. Buneo CA, Jarvis MR, Batista AP, Andersen RA. Direct visuomotor transformations for reaching. *Nature*. 2002;416:632–636.
82. Buneo CA, Andersen RA. The posterior parietal cortex: sensorimotor interface for the planning and online control of visually guided movements. *Neuropsychologia*. 2006;44:2594–2606.
83. Desmurget M, Epstein CM, Turner RS, Prablanc C, Alexander GE, Grafton ST. Role of the posterior parietal cortex in updating reaching movements to a visual target. *Nat Neurosci*. 1999;2:563–567.
84. Lin X, Ding K, Liu Y, Yan X, Song S, Jiang T. Altered spontaneous activity in anisometropic amblyopia subjects: revealed by resting-state fMRI. *PLoS ONE*. 2012;7:e43373.
85. Wang T, Li Q, Guo M, et al. Abnormal functional connectivity density in children with anisometropic amblyopia at resting-state. *Brain Res*. 2014;1563:41–51.

Investigative Ophthalmology & Visual Science

Appendix A: Participant Information

Table A1. Characteristics of the Amblyopic Participants

No.	Sex	Age	Type	Correction	SA	VA	Treatment	Experienced
A1	M	29	Aniso	+4.75DS	200	0.32	Refractive correction, patching, vision therapy	Yes
				+3.00DS		0.3		
A2	F	27	Aniso	–2.50DS/–0.50DC × 42°	200	–0.1	Refractive correction	Yes
				+2.25DS/–0.25DC × 175°		0.2		
A3	M	29	Isoam	+6.50DS/–2.00DC × 5°	200	0.25	Refractive correction	No
				+7.00DS/–2.00DC × 170°		0.23		
A4	M	18	Aniso	Plano	400	–0.1	Refractive correction, patching, vision therapy	Yes
				+3.25DS/–0.75DC × 165°		0.1		
A5	M	30	Aniso	–7.00DS/–0.75DC × 135°	400	0.4	Refractive correction	Yes
				–5.00DS/–0.75DC × 58°		0.0		
A6	M	25	Aniso	–1.75DS/–0.50DC × 160°	200	–0.1	Refractive correction, patching	Yes
				+2.75DS/–1.50DC × 167°		0.4		
A7	M	19	Aniso	–8.25DS/–2.50DC × 8°	400	0.0	Refractive correction	Yes
				–0.25DS/–2.50DC × 174°		0.6		
A8	F	22	Aniso	+0.25DS/–0.25DC × 65°	200	0.0	Refractive correction, patching, vision therapy	No
				+2.25DS/–0.25DC × 35°		0.5		
A9	M	25	Aniso	–0.75DS	NA	0.0	Refractive correction	No
				+1.00DS/–3.00DC × 160°		0.2		
A10	F	26	Aniso	+1.50DS	NA	0.2	Refractive correction, patching	Yes
				–1.50DS		0.0		
A11	F	19	Aniso	–2.00DS	NA	–0.1	Refractive correction, patching, vision therapy	Yes
				+3.00DS		0.2		
A12	F	29	Aniso	Plano	200	0.0	None	Yes
				+1.75DS		0.2		
A13	F	23	Aniso	–2.50DS	80	–0.1	Refractive correction, patching, vision therapy	Yes
				+2.00DS		0.2		
A14	M	29	Aniso	+4.00DS	400	0.42	Refractive correction	Yes
				+2.25DS		0.1		
A15	M	24	Aniso	–4.50DS	200	–0.1	Refractive correction, patching	Yes
				+5.50DS		0.4		
A16	F	31	Aniso	+3.75DS/–1.50DC × 155°	400	0.5	None	Yes
				–0.50DS		0.0		
A17	F	24	Aniso	–1.00DS/–0.50DC × 90°	NA	0.0	Refractive correction, patching, vision therapy	Yes
				+1.75DS/–1.75DC × 65°		0.2		
A18	M	22	Aniso	+3.50DS/–1.25DC × 10°	200	0.3	Refractive correction, patching	No
				+1.25DS/–0.75DC × 172°		–0.1		
A19	M	24	Aniso	–1.00DS	400	–0.1	Refractive correction, patching	Yes
				+4.75DS		0.6		
A20	M	31	Aniso	+1.75DS/–1.75DC × 159°	NA	0.3	None	No
				+3.25DS/–3.00DC × 29°		0.4		
A21	M	27	Isoam	+6.25DS/–2.50DC × 150°	NA	0.1	Refractive correction	Yes
				+6.50DS/–3.75DC × 17°		0.3		
A22	F	28	Aniso	–0.50DS	400	–0.1	Refractive correction, patching	Yes
				+4.50DS/–0.75DC × 100°		0.5		
A23	M	29	Aniso	+1.25DS/–0.75DC × 10°	400	0.4	Refractive correction, patching	Yes
				–5.00DS		–0.1		
A24	M	27	Aniso	–1.00DS	200	–0.1	Refractive correction, patching	Yes
				+2.50DS/–0.50DC × 30°		0.5		

A1–A15 participated in experiment 1; A2, A3, A5, A6, A7, A8, A12, A13, A14, and A16–A21 participated in experiment 2; and A2, A3, A5, A6, and A22–A24 participated in experiment 3. Treatment includes refractive correction, patching, and vision therapy. Aniso, anisometropia; Isoam, isoametropic; NA, not measured; SA, stereoacuity in arcmin; VA, visual acuity in logMAR.

Investigative Ophthalmology & Visual Science

Table A2. Characteristics of the Normal Participants

No.	Sex	NDE	Age	Correction	SA	VA	Experienced
N1	F	RE	25	–3.75DS	40	–0.1	Yes
				–3.75DS		–0.1	
N2	M	RE	24	–0.75DS/–0.25DC × 90°	40	–0.1	Yes
				–0.50DS/–0.50DC × 90°		–0.1	
N3	F	RE	26	–3.25DS/–0.50DC × 180°	40	0.0	Yes
				–4.00DS		0.0	
N4	F	LE	28	–4.00DS	40	–0.1	Yes
				–3.25DS		0.0	
N5	M	RE	25	–3.00DS/–0.75DC × 8°	40	0.0	Yes
				–2.25DS/–0.75DC × 4°		0.0	
N6	F	LE	28	Plano	40	–0.1	No
				–0.25DS		0.0	
N7	F	LE	25	–3.00DS	40	–0.1	Yes
				–3.00DS		–0.1	
N8	M	LE	25	–3.25DS	40	0.0	Yes
				–3.25DS/–0.50DC × 15°		0.0	
N9	M	LE	24	–1.00DS/–1.00DC × 90°	40	0.0	Yes
				–1.25DS/–0.75DC × 80°		0.0	
N10	F	LE	23	–3.50DS	40	0.0	Yes
				–3.00DS		0.0	
N11	F	RE	25	–2.75DS	40	0.0	Yes
				–3.25DS		0.0	
N12	F	LE	23	–2.00DS	40	–0.1	Yes
				–1.50DS		–0.1	
N13	F	LE	25	–0.50DS	40	0.0	Yes
				–1.00DS		0.0	
N14	M	LE	24	–0.75DC × 88°	40	0.0	No
				–0.75DS/–0.25DC × 84°		0.0	
N15	F	LE	28	–4.50DS	40	–0.1	Yes
				–4.25DS		0.0	
N16	F	LE	26	–1.00DS	40	–0.1	Yes
				–1.75DS		–0.1	
N17	M	RE	30	–3.75DS	40	0.0	Yes
				–3.50DS/–0.50DC × 170°		0.0	
N18	M	LE	23	–4.50DS/–0.25DC × 30°	40	0.0	Yes
				–4.25DS/–0.25DC × 165°		0.0	
N19	F	RE	28	–1.00DS/–1.00DC × 77°	40	0.0	Yes
				–1.00DS/–0.50DC × 140°		0.0	
N20	F	LE	26	Plano	40	–0.1	Yes
				Plano		–0.1	
N21	F	RE	29	–3.50DS/–0.75DC × 40°	40	–0.1	Yes
				–4.00DS		–0.1	
N22	M	LE	28	+0.50DS	40	0.0	Yes
				–0.75DS/–0.25DC × 100°		0.0	

N1–N15 participated in experiment 1; N2–N6, N9, and N14–N22 participated in experiment 2; and N2, N3, N5, N15, N18, N19, and N22 participated in experiment 3. LE, left eye; NDE, nondominant eye is the test eye; RE, right eye; SA, stereoacuity in arcmin; VA, visual acuity in logMAR.

Investigative Ophthalmology & Visual Science

Appendix B: The Spectrum and Location Uncertainty of the Stimulus

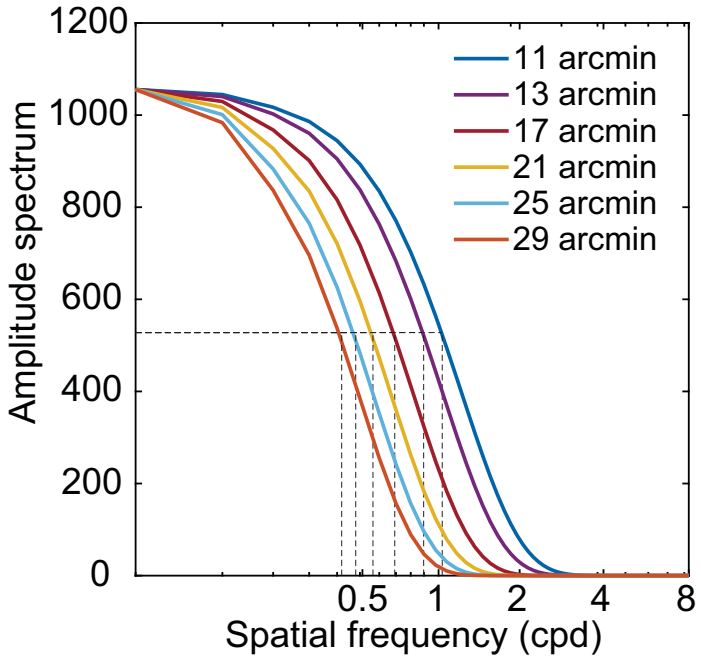

Figure B1. The amplitude spectrum of the target at different sizes is plotted in different colors. Vertical *dashed lines* indicate the spatial frequency that corresponds to the half of the maximum amplitude for each size.

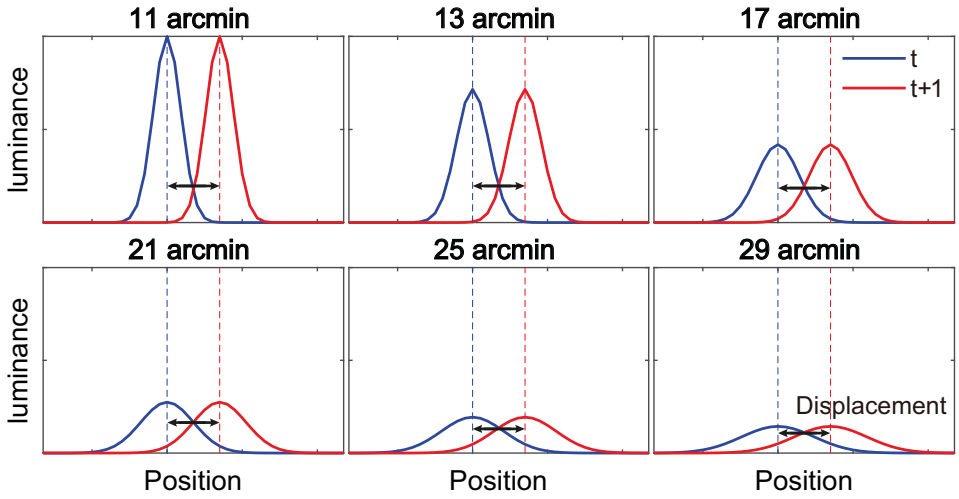

Figure B2. The cross sections of the target at two consecutive locations during random walk (t frame and $t + 1$ frame). The luminance of the target was varied with its size so that the luminous flux (the volume under the Gaussian) was constant for all target sizes. The observer's performance was determined by the ratio between the step size of the random walk and the uncertainty of the target location. This design used the property that, for Gaussian targets, the probability of the target center being at a specific location is directly proportional to the luminance value at that location. The constant luminous flux is equivalent to the equal total probability of the Gaussian for all target conditions. As the target size increases, the tracking becomes more difficult.

Appendix C: CSF Data of Participants

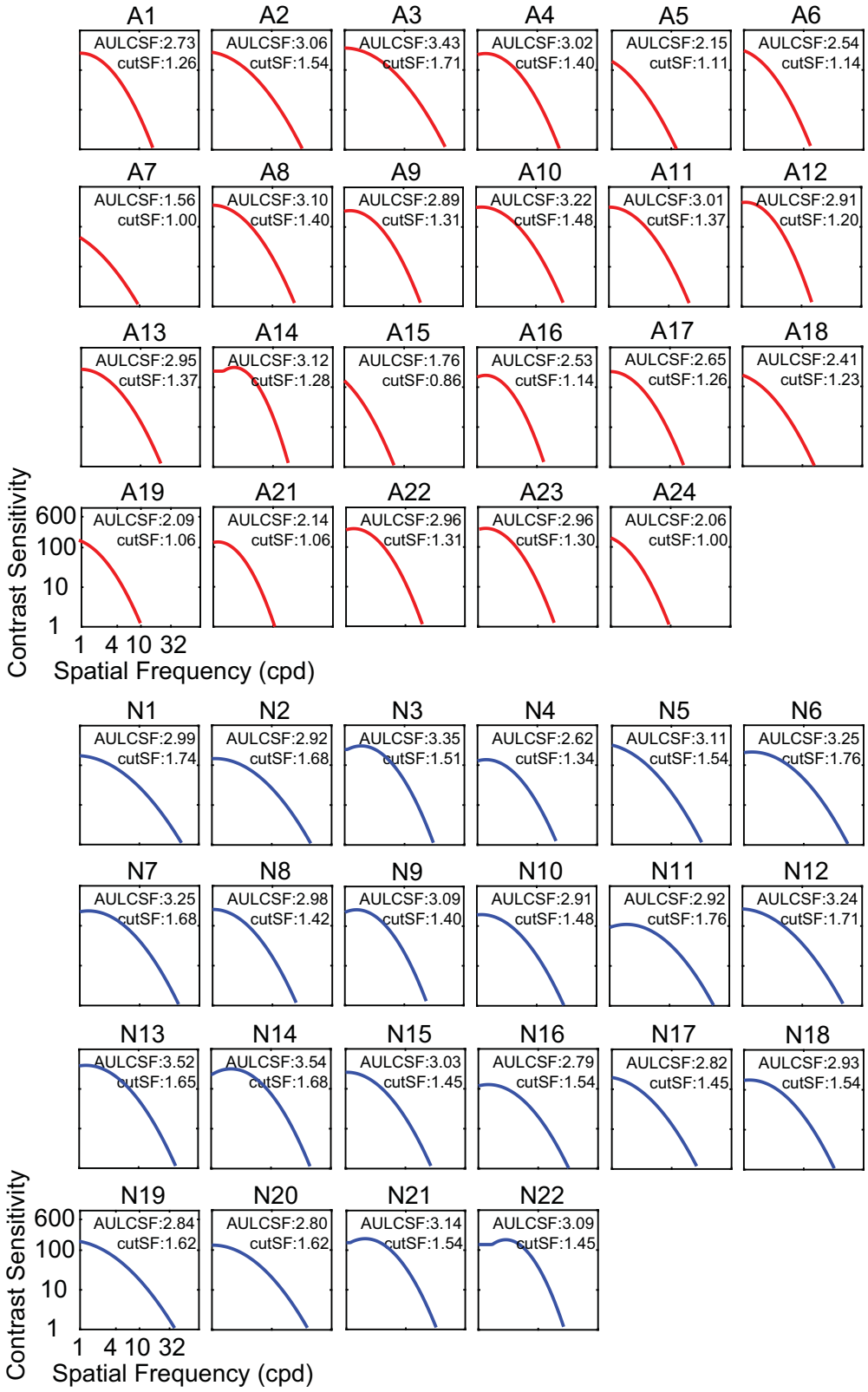

Figure C1. CSF of each participant. The AULCSF and cutSF are also shown for each participant. *Red*: amblyopic participants; *blue*: normal participants.

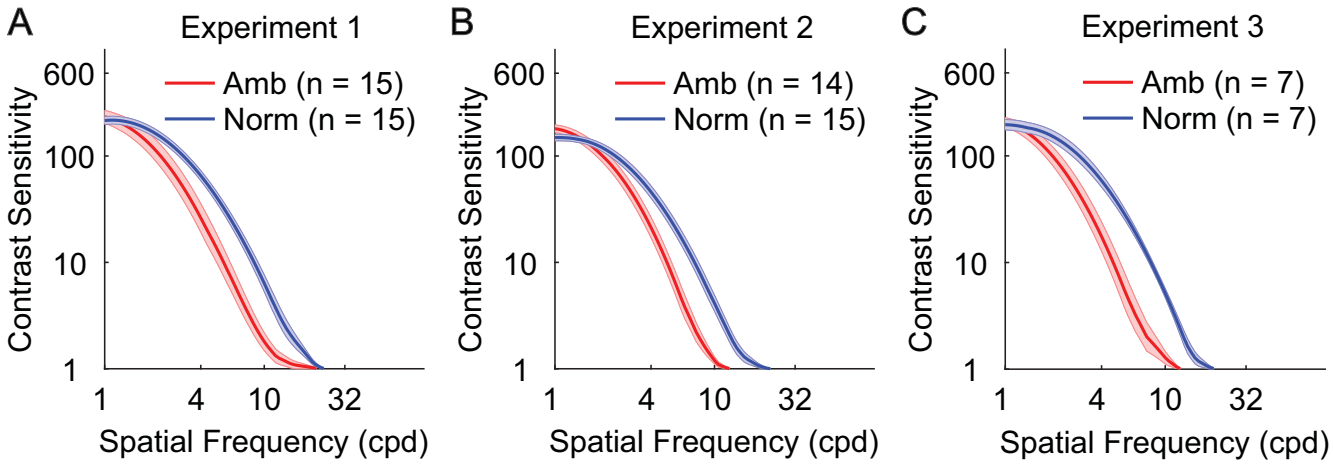

Figure C2. The average contrast sensitivity functions of the amblyopic and normal groups in experiment 1 (**A**), experiment 2 (**B**), and experiment 3 (**C**) are shown in separate panels. *Red and blue curves* represent the amblyopic and normal groups, respectively. *Shaded areas* represent ±1 standard error.

Appendix D: The Goodness of Fit of the Tracking Kernel

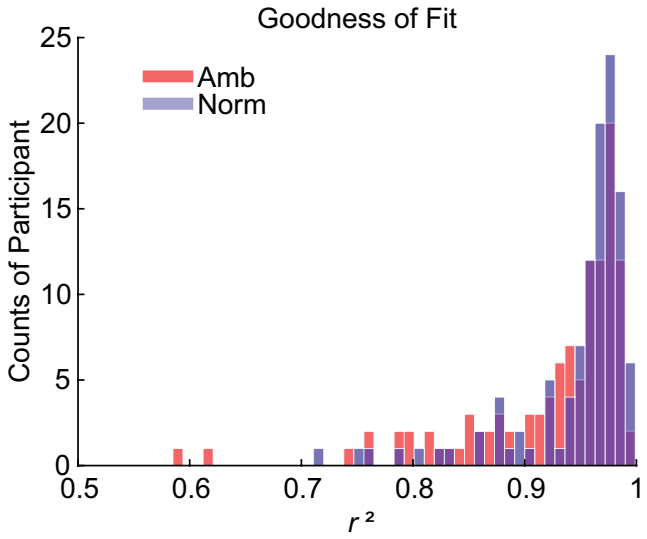

Figure D1. The histogram of the r^2 of the best-fit model pooled over three experiments for the amblyopic (*red*) and normal groups (*blue*).